Fracture Mechanics of Concrete and Concrete Structures -
Recent Advances in Fracture Mechanics of Concrete - B. H. Oh, et al.(eds)

Acoustic and electromagnetic emissions related to stress-induced cracks

G. Lacidogna, A. Manuello & A. Carpinteri
Politecnico di Torino, Torino, Italy

G. Durin, G. Niccolini, A. Schiavi, A. Agosto
National Research Institute of Metrology – INRiM, Torino, Italy

ABSTRACT: The mechanical behaviour of concrete and rocks samples loaded up to their failure is analyzed by Acoustic Emission (AE) and Electromagnetic Emission (EME). All specimens were tested in compression at a constant displacement rate and monitored by piezoelectric (PZT) transducers for AE data acquisition. Simultaneous investigation of magnetic activity was performed by a measuring device calibrated according to metrological requirements. In all the considered cases, the presence of AE events has been always observed during the damage process, whereas it is very interesting to note that the magnetic signals were generally observed only in correspondence of sharp stress drops or the final collapse.

1 INTRODUCTION

The present research focuses on Acoustic Emission (AE) and Electromagnetic Emission (EME) detected during laboratory compression tests on concrete and rocks specimens. We investigated their mechanical behaviour up to failure by the AE and EME due to micro- and macro-crack growth.

Among the tested specimens, a concrete sample was analyzed by applying to its surface both piezoelectric (PZT) transducers for detection of high-frequency AE waves, and PZT accelerometric transducers for detection of low-frequency AE (elastic emission, or ELE) (Schiavi et al. 2009). Besides the high-frequency acoustic emissions (AE), the emergence of low-frequency elastic emissions (ELE) just before the failure describes the transition from diffused micro-cracking to localized macro-cracks which characterizes the failure in brittle materials.

For all the specimens, a simultaneous analysis of magnetic activity was performed by a measuring device calibrated according to metrological requirements. In all the considered specimens, the presence of AE events has been always observed during the damage process, whereas it is very interesting to note that the EME were generally observed only in correspondence of sharp stress drops or the final collapse (Lacidogna et al. 2009).

The experimental evidence confirms AE and EME signals as collapse precursors in materials like concrete and rocks. As AE and EME coincide when certain types of rocks fail, the influence of EM fields on the AE transducers has been previously evaluated in order to be minimized. Given a fracture process, the AE activity behaves as fracture precursor, since it precedes EME events, which accompany stress drops and related discontinuous fracture advancements. While the mechanism of AE is fully understood, being provided by transient elastic waves due to stress redistribution following fracture propagation (Kaiser 1950, Pollock 1973, Ohtsu 1996, Carpinteri et al. 2005, 2007, 2008), the origin of EME from fracture is not completely clear and different attempts have been made to explain it.

2 ELASTIC WAVE PROPAGATION IN HIGH AND LOW FREQUENCY RANGES

During the damage of a brittle material in compression, micro- and macro-cracks generate elastic waves of frequency and wavelength related to the size of the cracks. In fact, a newly formed crack can be considered as a sort of pendulum of length L (representing the crack length) and oscillation frequency f (representing the frequency of the emitted elastic wave), with $f \propto L^{-1/2}$. Following this analogy, micro-cracks emit elastic waves of high frequency and short wave-length (AEs), while macro-cracks taking place at failure are characterized by lower frequencies of oscillation and larger wave-lengths (ELEs).

In the case of AE, the longitudinal wave propagation is due to the oscillations of material particles around their equilibrium positions (Figure1a). As the collapse is approaching, macro-cracks are created and some macroscopic portions of the specimen are subjected to sudden and appreciable changes of their spatial locations. The impulse generated by a macro-crack involves a perturbation (ELE) able to "shake" the whole specimen with relevant oscillation amplitudes and low oscillation frequencies (Figure1b). These oscillations, detected at the very last stages of the test, are analogous to "shock waves" for which the medium moves from the equilibrium position (Johnson 1999, Larcher 2009). Based on these considerations, it is therefore possible to distinguish the effects of the two different emissions, AE and ELE, and analyze them separately.

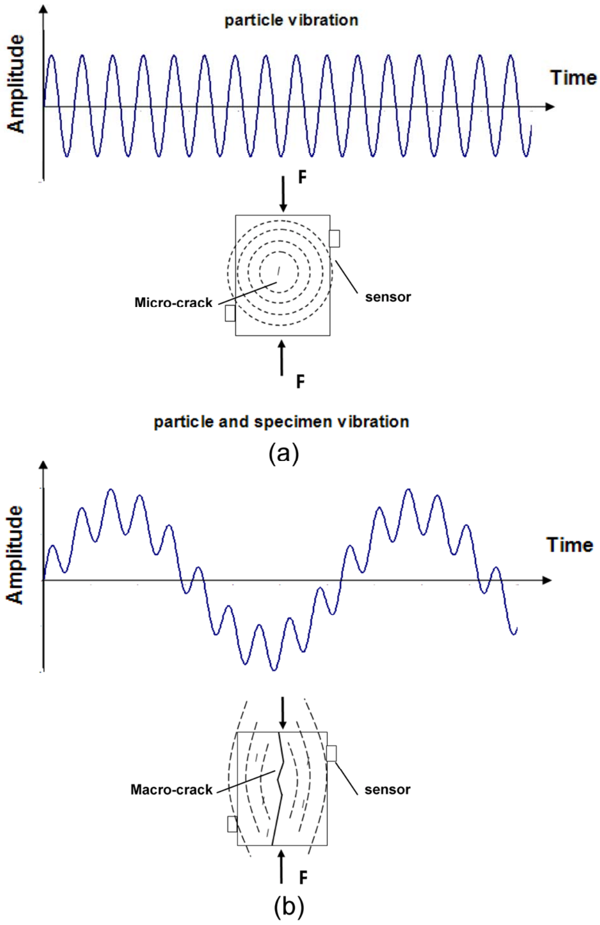

Figure 1. (a) Schematic representation of AE due to particle vibration around their equilibrium position. (b) Schematic representation of ELE due to relevant oscillations of the entire specimen.

3 MODELS FOR EME

An explanation of the EME origin was related to dislocation phenomena (Misra 1977, 1978), which however are not able to explain EME from fracture in brittle materials where the motion of dislocations can be neglected (Frid et al. 2003). The weakness of the "dislocation movement hypothesis" was confirmed in some experiments showing that the EME amplitude increased with the brittleness of the investigated materials (Jagasivamani & Iyer 1988). In brittle materials the fracture propagation occurs suddenly and it is accompanied by abrupt stress drops in the stress-strain curve related to sudden loss in the specimen stiffness.

Another relevant attempt to explain the EME origin was made through the "capacitor model", where EME is assumed to be caused by net charges of opposite sign appearing on the vibrating faces of opening cracks (Miroshnichenko & Kuksenko 1980, O'Keefe & Thiel 1995). This model is not widely accepted since an accelerated electric dipole created by charged opening cracks apparently does not explain EME from shearing cracks, which indeed are experimentally observed (Frid et al. 2003). However, the general validity of this model can be maintained, since a certain separation between charged faces is guaranteed even in shear fractures.

Frid et al. (2003) and Rabinovitch et al. (2007) recently proposed a model of the EME origin where, following the rupture of bonds during the cracks growth, mechanical and electrical equilibrium are broken at the fracture surfaces with creation of ions moving collectively as a surface wave on both faces. Lines of positive ions on both newly created faces (which maintain their charge neutrality unlike the capacitor model) oscillate collectively around their equilibrium positions in opposite phase to the negative ones (see Fig. 2). The resulting oscillating dipoles created on both faces of the propagating fracture act as the source of EME. According to this model, the EME amplitude increases as long as fracture propagates, since the rupture of new atomic bonds contributes to the EME. When fracture stops, the waves and the EME decay by relaxation.

Since larger fracture advancements produce larger stress drops, this model agrees with the results in compression tests on rock specimens obtained by Fukui et al. (2005), which establish a relationship of proportionality between stress drop and intensity of related EME.

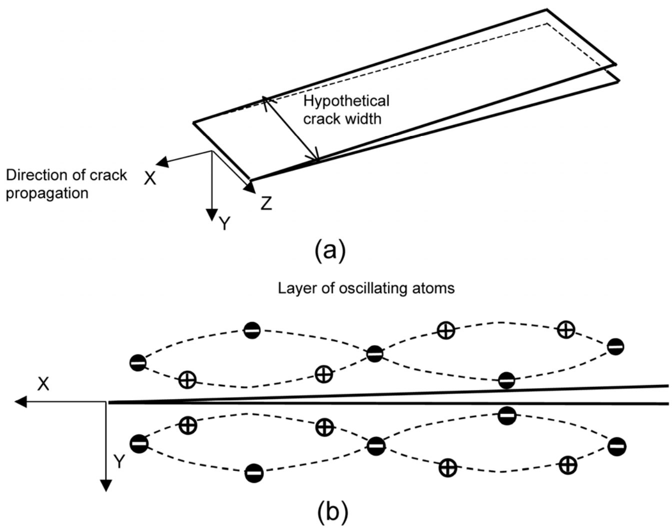

Figure 2. Picture of crack propagation and crack surfaces at a specific time. Crack surfaces are in the xz plane and the crack propagates in the x direction (a). Schematic representation at a specific time of surface waves propagating on the two newly formed crack surfaces. Layers of atoms move together generating surface vibrational waves on each face, where positive charges vibrate in opposite phase to the negative ones (b).

4 EXPERIMENTAL SET-UP

Four specimens made of different brittle materials (Concrete, Syracuse Limestone, Carrara Marble, and Green Luserna Granite) were examined in this study (Fig. 3) (Lacidogna et al. 2009). They were subjected to uniaxial compression using a Baldwin servo-controlled hydraulic testing machine with a maximum capacity of 500 kN and load measurement accuracy of ± 1.0%. This machine is equipped with control electronics which makes it possible to carry out tests in either load control or displacement control. Each test was performed in piston travel displacement control by setting constant piston velocity. The test specimens were arranged in contact with the press platens without any coupling materials, according to the testing modalities known as “test by means of rigid platens with friction”. The tested materials, shapes and sizes of the specimens, and the employed piston velocities are listed in Table 1.

Table 1. Materials, shapes, sizes of the tested specimens, and piston velocities.

Specimen	Material	Shape	Volume cm^3	Piston velocity $m\ s^{-1}$
P1	Concrete	Cubic	10×10×10	0.5×10^{-6}
P2	Syracuse Limestone	Cylindrical	$\pi\times2.5^2\times10$	1.0×10^{-6}
P3	Carrara Marble	Prismatic	6×6×10	0.5×10^{-6}
P4	Green Luserna Granite	Prismatic	6×6×10	2.0×10^{-6}

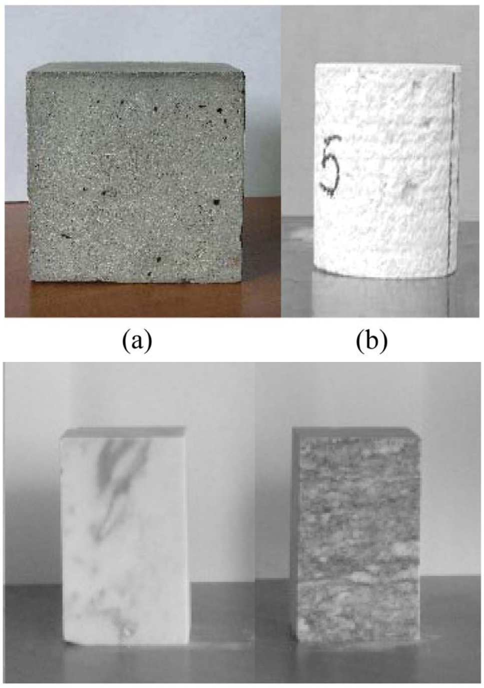

(a) (b) (c) (d)

Figure 3. Views of test specimens: (a) Concrete, (b) Syracuse Limestone, (c) Carrara Marble, and (d) Green Luserna Granite.

5 AE AND EME MEASUREMENTS

The acoustic emission emerging from the compressed specimens was detected applying to the sample surface a piezoelectric (PZT) transducer, sensitive in the frequency range from 50 to 500 kHz for detection of high-frequency acoustic emission (AE). As stated in the Introduction, during the test on specimen P1 (see Table 1) also a PZT accelerometric transducer, sensitive in the frequency range from 1 to 10 kHz, was used for detection of low-frequency acoustic emission (elastic emission, or ELE) (Schiavi et al. 2009).

The EM emission was detected using an isotropic probe calibrated according to metrological requirements at the National Research Institute of Metrology (Turin, Italy) for measuring the magnetic component of EM fields. The adopted device (Narda ELT-400 exposure level tester) works in the frequency range between 10 Hz and 400 kHz, the measurement range is between 1 nT and 80 mT, and the three-axial measurement system has a 100 cm^2 magnetic field sensor for each axis. This device was placed 1 m away from the specimens.

The outputs of the PZT transducer and the magnetic tester were connected to a DL708 Yokogawa oscilloscope (10 MSa s^{-1}) in order to acquire simultaneously AE and EME signals associated with the same fracture event. Data acquisition of the EME signals was triggered when the magnetic field exceeded the threshold fixed at 0.2 μT after preliminary measurements to filter out the magnetic noise in the laboratory. The recorded AE and EME signals were related to the time history of the load applied to the specimens.

6 TEST RESULTS

All specimens were tested in compression up to failure, showing a brittle response with a rapid decrease in load-carrying capacity when deformed beyond the peak load (Figs. 4-7). Experimental evidence indicates the presence of AE and EME: an increasing AE activity is always detected as the load increases, while EME is only observed when abrupt stress drops occur. In the following we focus on specimens P1 and P2 (Figs. 4, 5), representing two typical examples of catastrophic and quasi-brittle behaviours (Hudson et al. 1972, Carpinteri 1986, 1989, 1990).

The Concrete specimen P1 exhibits a very steep softening branch (descending part of the stress-strain curve), which is said “snap-back” or catastrophic behaviour (Fig. 4) (Carpinteri 1986, 1989, 1990). On the other hand, the Syracuse Limestone, specimen P2, retains considerable strength beyond the peak load. Despite their different mechanical behaveiours, specimens P1 and P2 both generate EME during sharp stress drops: P1 only at the peak load, whereas P2 even at the two intermediate stress drops occurred before the peak load. No further EME signals were detected in the post-peak region (Fig. 5).

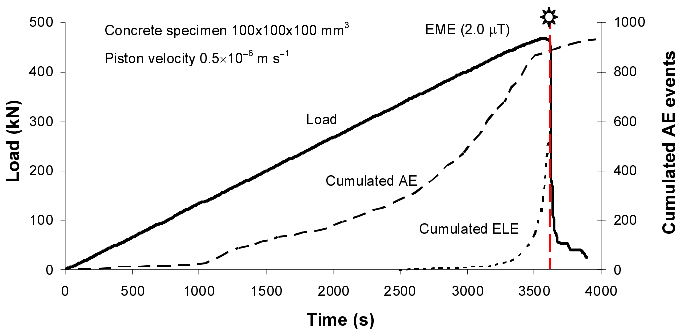

Figure 4. Load vs. time curve of the Concrete specimen P1 (bold line). The dashed line and the dotted line represent the cumulated number of respectively AE (high-frequency) and ELE (low-frequency). The star on the graph shows the moment of EME event with a magnetic component of 2.0 μT.

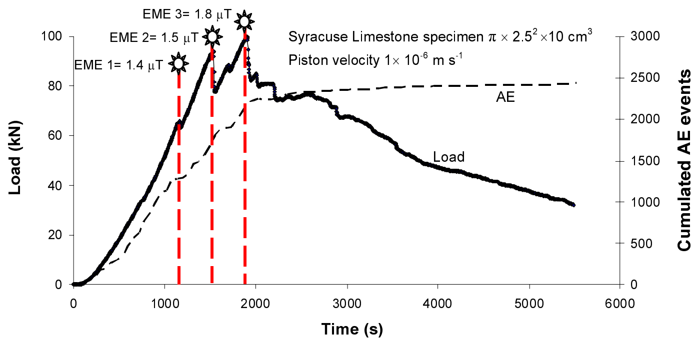

Figure 5. Load vs. time curve of the Syracuse Limestone specimen P2 (bold line). The dashed line represents the cumulated number of AE. The stars on the graph show the moments of EME events with magnetic component comprised between 1.4 and 1.8 μT.

The Concrete specimen P1, subjected to AE, ELE and EME monitoring, is characterized by a load vs. time diagram almost linear up to failure. At 70% of the peak load, we observed a significant increase in the AE rate (the slope of the dashed line in Figure 4), and the appearance of ELE (the dotted line in Figure 4). At 90% of the peak load, the ELE rate increases dramatically while the AE rate suddenly drops down. This evidence clearly indicates the transition from a microcracking-dominated damage process (revealed by the AE occurrence) to a process dominated by the propagation of a few large cracks and ELE. Therefore, AE and ELE are both fracture precursors, while an EME event (with magnetic component of 2 μT) was detected just in correspondence of the abrupt stress drop occurred at the specimen collapse (i.e., at the peak load).

The Syracuse Limestone specimen P2, subjected to AE and EME monitoring, is characterized by a more complex load vs. time diagram due to the heterogeneity of limestone. We observed three stress drops followed by as many drops in the AE rate, suggesting momentary relaxation after sudden crack advancements (Fig. 5).

Even in this case, we detected three EME events (with magnetic components ranging between 1.4 and 1.8 μT) in correspondence of each observed stress drop until the peak load is reached. The first stress drop occurred at 70% of the peak load, and the last one occurred at the peak load. It is worth noting that the EME intensity apparently does not depend, or depends weakly, as observed in Fukui et al. (2005), on the stress drop. In fact, similar magnetic components are associated to different stress drops. In particular, the first stress drop is clearly the smallest.

During the post-peak stage, i.e., softening branch in the load vs. time diagram, no further EME signals were detected. In fact, at the peak load the fracture is completely formed and the subsequent stages are characterized only by opening of the fracture surfaces. According to the model proposed by Frid et al. (2003) and Rabinovitch et al. (2007), this means that no newly broken atomic bonds can contribute to EME.

Summarising, the AE activity behaves as fracture precursor since it precedes EME events, which accompany stress drops and related discontinuous fracture advancements (see also the response of specimens P3 and P4, reported in Figs. 6, 7).

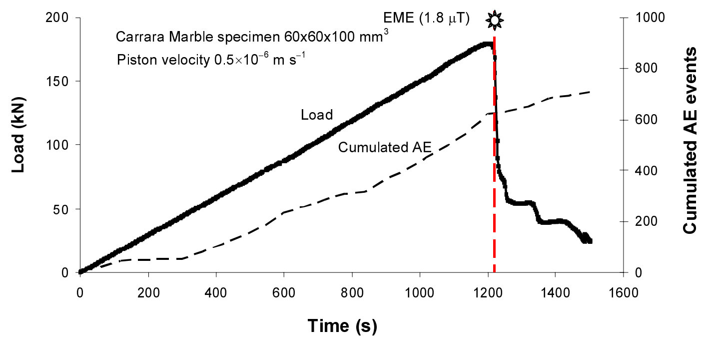

Figure 6. Load vs. time curve of the Carrara Marble specimen P3 (bold line). The dashed line represents the cumulated number of AE. The star on the graph shows the moment of EME event (magnetic component of 1.8 μT).

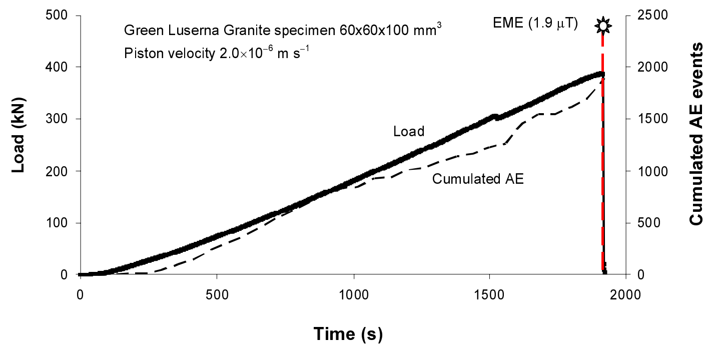

Figure 7. Load vs. time curve of the Green Luserna Granite specimen P4 (bold line). The dashed line represents the cumulated number of AE. The star on the graph shows the moment of EME event (magnetic component of 1.9 μT).

7 DETAILED AE DATA ANALYSIS ON SPECIMEN P1

First of all, the global level of the background-noise vibration in the LF-range, between 1 kHz and 10 kHz, has been evaluated in laboratory. In this frequency range, the mechanical noise has an average value of about 62±2 dB (referred to 1 $\mu m/s^2$). In particular, it is possible to distinguish three different peak levels corresponding to 2.5 kHz, 5.3 kHz, and 5.8 kHz, with an almost constant peak level between 50 dB and 53 dB (Fig. 8). These signals can be recognized as due to the servo-hydraulic press noise. Nevertheless, it is possible to note that the background-noise has a negligible influence if compared to ELE signals. The ELE acceleration spectral levels are between 80 dB and 120 dB.

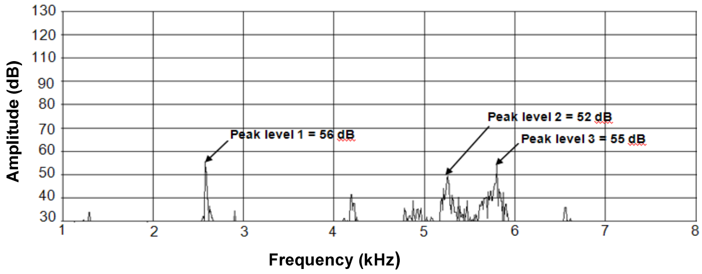

Figure 8. Global level of the background-noise vibration.

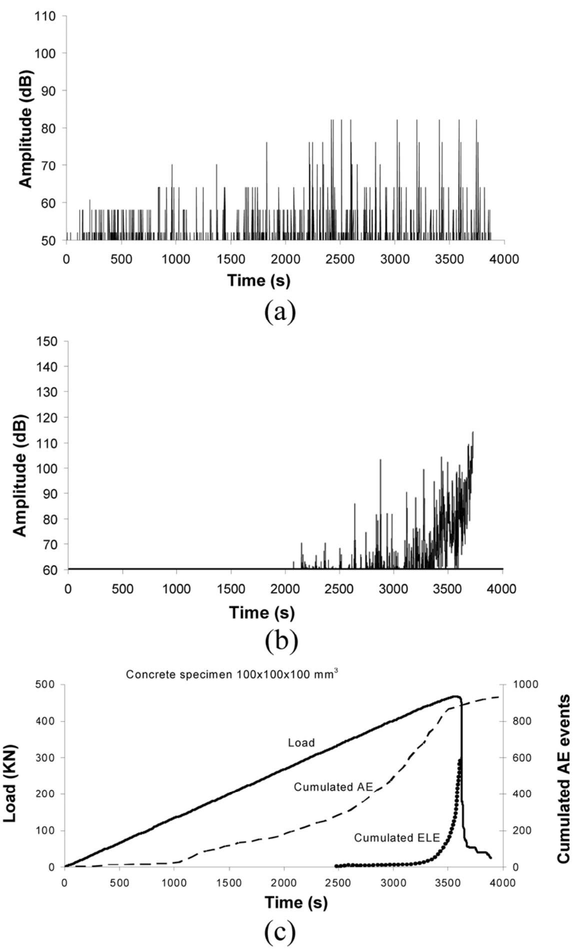

Figure 9. (a) AE and (b) ELE time history on Concrete specimen P1. (c) Load vs. time together with cumulative AE and ELE counts for each minute of the testing time.

In Figures 9a, 9b the amplitude level time histories of AE and ELE on Concrete specimen P1 are reported. AE have been detected since the beginning of the test (Fig. 9a), while the early ELE have been detected 2200 s later (Fig. 9b). The late appearance of ELE, their increasing rate (number of ELEs per unit time), and the increase in the amplitude levels are signatures of specimen damage evolution. In Figure 9c load vs. time, together with cumulative AE and ELE counts (for each minute of the testing time), are depicted.

Cumulative AE counts increase, very slowly at first, then proportionally to the load up to 2500 s. After this time, AE rate increases notably reaching a peak in the proximity of the highest load (3500 s). The AE rate increase (observed in the time window: 2500 s - 3500 s) is in correspondence to a dramatic increase in ELE counts. In this phase (3500 s - 3700 s), just before the collapse condition, ELE counts grow more quickly than AE counts and a larger number of macro-cracks is created (Fig. 9c).

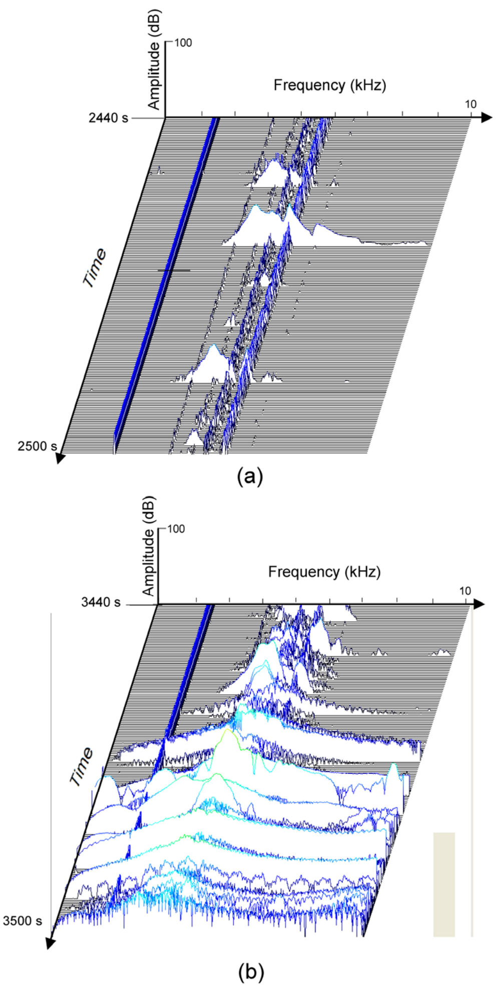

Figure 10. (a) An initial and (b) a final phase of ELE activity during the test.

Figure 10a represents the initial phase of ELE activity characterized by sporadic signals with energy content concentrated in a narrow frequency interval. Similarly in Figure 10b the phase just before the specimen collapse is represented. In this case a greater number of ELEs is detected with more significant energy content in a wide frequency range, probably extending beyond the observation window size. Figure 11 shows the spectral contents of two ELEs at 2757 s and 3424 s. In Figure 11a the spectrum has a peak level equal to 62 dB and a global level of about 77.1 dB. In Figure 11b the spectrum has a peak level equal to 100 dB and a global level of about 115.0 dB. Based on these data, it is possible to describe macro-crack effects in terms of released energy, measuring the local acceleration in the accelerometer point of application.

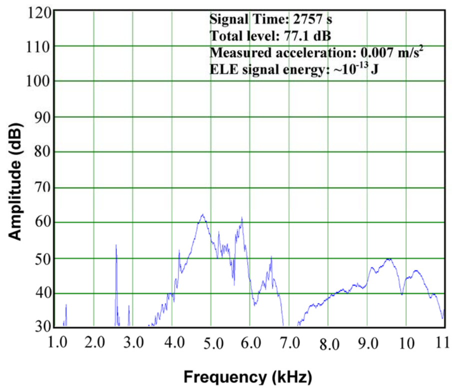

(a)

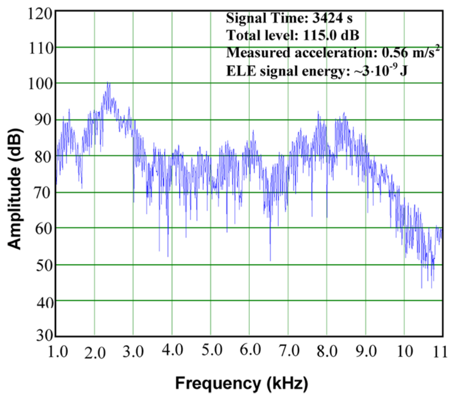

(b)

Figure 11. Spectral contents of two ELEs measured at 2757 s and 3424 s.

In Figure 12, the peak frequency and amplitude of each ELE signal are reported. By means of these diagrams, it is possible to investigate the specimen damage evolution. The time dependence of the peak frequencies and amplitudes are split into two parts identifying the two different stages in the damage evolution.

In the first part, the peak frequencies are between 4.8 kHz and 5.8 kHz (Fig. 12a), while the peak amplitudes are between 60 dB and 75 dB (Fig. 12b). Though the number of macro-cracks increases, macroscopic collapse is not reached.

On the contrary, in the second phase a sudden decay in the frequency domain and an abrupt increase in the amplitude levels indicate that macro-cracks coalesce to generate the final rupture surfaces (Figs. 12a, 12b). Therefore, the peak frequencies of ELE signals decrease with increasing damage level. These results imply that the ELE frequency decay can be assumed as a valid indicator of the damage evolution.

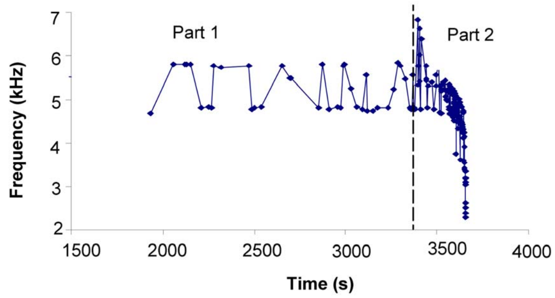

(a)

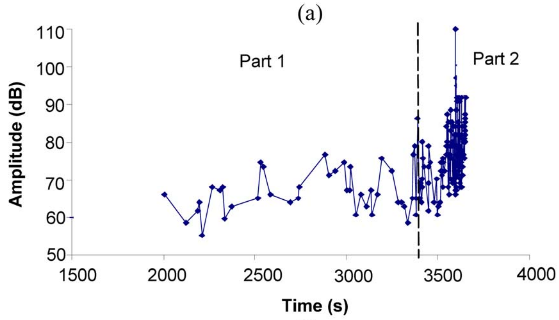

(b)

Figure 12. (a) Time history of peak frequencies and (b) peak amplitudes of ELE signals.

8 AE AND ELE FREQUENCY-MAGNITUDE STATISTICS

By analogy with seismic phenomena, the magnitude of AE and ELE events can be defined as follows (Colombo et al. 2003, Rao & Lakschmi 2005, Carpinteri et al. 2005, 2008, 2009a, 2009b):

$$m = Log_{10} A_{\max} + f(r), \tag{1}$$

where A_{max} is the amplitude of the signal expressed in dB (referred to 1 mV for the AEs and to 1 μm/s^2 for the ELEs), and $f(r)$ is a correction term which accounts for the amplitude attenuation with the distance r between the source and the sensor. In seismology, the Gutenberg-Richter (GR) empirical law (Richter 1958):

$$Log_{10} N(\geq m) = a - bm, \quad \text{or} \quad N(\geq m) = 10^{a-bm}, \tag{2}$$

is one of the most widely used statistical relationships to describe the scaling properties of seismicity.

In Equation (2), N is the cumulative number of earthquakes with magnitude $\geq m$ in a given area and within a specific time period, whilst a and b are positive constants depending on the considered area and time period. Equation (2) has been successfully used in the AE field to study the scaling laws of the amplitude distribution of AEs. This approach emphasizes the similarity between damage phenomena in the materials and the seismic activity in a given region of the Earth Crust, extending the applicability of the GR law to Damage Mechanics. The b-value in Equation (2) changes systematically during the different stages of the damage process and therefore can be used to detect the evolution of damage (Colombo et al. 2003, Rao & Lakschmi 2005, Carpinteri et al. 2005, 2008, 2009a, 2009b).

The GR law can be written in an alternative form (Rundle et al. 2003):

$$N(\geq L) = c L^{-2b}, \tag{3}$$

where N is the cumulative number of AE events generated by cracks having a characteristic length $\geq L$, c is a constant of proportionality, and $2b = D$ is the fractal dimension of the damage domain. It has been pointed out that this interpretation rests on the assumption of a dislocation model for the seismic source and requires that $2 \leq D \leq 3$, i.e., the cracks are distributed in a fractal domain comprised between a surface and the volume of the analysed region (Rundle et al. 2003). The cumulative distribution of Equation (3) is substantially identical to the one proposed by Carpinteri (1986, 1994), according to which the number of cracks with length $\geq L$ contained in a body is given by:

$$N^{*}(\geq L) \sim N_{tot} L^{-\gamma}. \tag{4}$$

In Equation (4), γ is a statistical exponent reflecting the disorder, i.e., the dispersion of the crack length distribution, and N_{tot} is the total number of cracks contained in the body. From Equations (3) and (4), we find that $2b = \gamma$. During the formation of the final fracture, cracks concentrate in a narrow band to form the final fracture surface. In this case, as shown by Carpinteri (1986) and Carpinteri et al. (2005, 2008, 2009a, 2009b), the self-similarity condition entails $\gamma = 2.0$. This exponent corresponds to the value $b = 1.0$, which is experimentally approached in structural elements during the final crack propagation.

Subdividing the loading process into different stages and calculating the related b-values, the relation $D = 2b$ permits to explain the evolution of damage in terms of progressive micro-cracks localization onto preferential domains. The trends of the b-value during the test on Concrete specimen P1 are shown in Figure 13 for both AE and ELE events. These trends are obtained by partitioning all detected events into groups of 100 events, and for each group the b-value has been calculated. With this method, already adopted in other damage analyses in structural concrete elements (Shiotani et al. 2000, Colombo et al. 2003), the testing time was subdivided into 6 and 10 intervals (600 and 1000 events) for ELE and AE time series, respectively.

Figure 13 shows that AEs generated during the early stages of loading give high b-values ($b > 1.5$). In particular, the b-values obtained by AE signals result to be greater than 1.8 during the first 2500 s. After 3000 s, the b-values reach 1.5 and tend to 1.0 at the end of the loading process. When the b-value is $\cong 1.5$ (Fig. 13), the cracks revealed by the AE signals are likely to be uniformly distributed throughout the specimen volume ($D = 2b \cong 3$). During the subsequent stages, micro-cracks coalesce to form macro-cracks and the b-value drops below 1.5 for both AE and ELE signals. The rapid decay of the b-value observed close to the peak load is a further confirmation to the catastrophic behaviour of the concrete specimen.

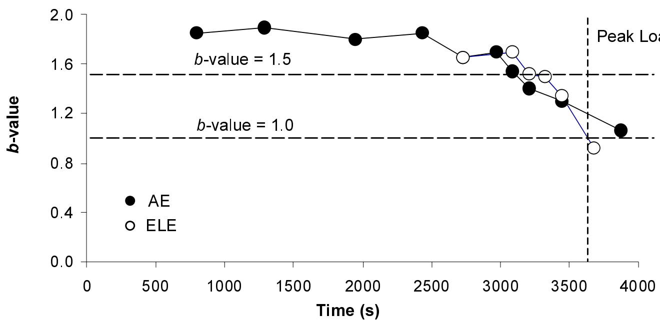

Figure 13. Trends of the b-value computed for AE and ELE signals.

9 CONCLUSIONS

It is widely reported that changes in geoelectric potential and anomalous radiation of geoelectromagnetic waves, especially in low-frequency bands, occur before major earthquakes. At the laboratory scale, similar phenomena have also been observed on rock specimens under loading. In this case, crack growth is accompanied by acoustic emission ultrasonic waves and by redistribution of electric charges.

First of all, we investigated the mechanical behaviour of rocks and concrete samples loaded in compression up to their failure by the analysis of AE and EME signals. In all the considered cases, the presence of AE events has been always observed during the damage process. Moreover, it is very interesting to note that the EME was generally observed only in correspondence to the sharp stress drops in the load vs. time diagrams. While the mechanism of AE is well understood, we adopted the model proposed by Frid et al. (2003) and Rabinovitch et al. (2007) to explain the EME origin, according to which EME is generated by oscillating dipoles created by ions moving collectively as a surface wave on both faces of the crack. This model accounts correctly for the occurrence of the abrupt stress drops in load vs. time diagrams due to sudden loss of specimen stiffness which accompanies discontinuous crack propagation (Hudson 1972, Carpinteri 1989, 1990).

Furthermore, the damage process occurring in a concrete specimen under compression was carefully studied by means of elastic wave propagation induced by crack growth. In particular, elastic emissions (ELE) in the frequency range 1-10 kHz were detected and analysed. In the last phases of the test, ELE count grows more quickly than AE count, revealing that a large number of macro-cracks is generated just before the collapse condition. These results imply that the sudden increase in the number and amplitude, and the simultaneous frequency decay of ELEs can be assumed as valid indicators of the impending failure. Furthermore, the achievement of the critical condition is also investigated through a synthetic parameter, the *b*-value. The rapid decay of *b*-value is a further confirmation to the steep decay in the load vs. strain curve after the peak load.

The experimental evidence confirms AE and EME signals as collapse precursors in materials like concrete and rocks. In particular, the high-frequency AE waves (50-500 kHz) are analysed during all stages of damage in compression, while the low-frequency waves ELE (1-10 kHz) are detected just before the collapse conditions. Finally, the EME are always observed during the sharp stress drops that precede the collapse. In this prospective, the opportunity to combine these monitoring techniques looks promising as a forecasting tool of damage from the structural to the geophysical scale.

ACKNOWLEDGEMENTS

The financial support provided by the European Union (EU) Leonardo da Vinci Programme, ILTOF Project, is gratefully acknowledged. Special thanks are due to Mr. V. Di Vasto of the Politecnico di Torino and to Dr. Eng. A. Pavoni Belli of the National Research Institute of Metrology – INRIM.

REFERENCES

Carpinteri, A. 1986. Mechanical Damage and Crack Growth in Concrete: Plastic Collapse to Brittle Fracture. Dordrecht: Martinus Nijhoff Publishers.

Carpinteri, A. 1989. Cusp catastrophe interpretation of fracture instability. Journal of the Mechanics and Physics of Solids 37: 567-582.

Carpinteri, A. 1990. A catastrophe theory approach to fracture mechanics. International Journal of Fracture 44: 57-69.

Carpinteri, A. 1994. Scaling laws and renormalization groups for strength and toughness of disordered materials. International Journal of Solids and Structures 31: 291-302.

Carpinteri, A., Lacidogna G. & Niccolini G. 2005. Critical behaviour in concrete structures and damage localization by acoustic emission. Key Engineering Materials 312: 305-310.

Carpinteri, A., Lacidogna, G., Niccolini, G. & Puzzi, S. 2008. Critical defect size distributions in concrete structures detected by the acoustic emission technique. Meccanica 43: 349-363.

Carpinteri, A., Lacidogna, G., Niccolini, G. & Puzzi, S. 2009a. Morphological fractal dimension versus power-law exponent in the scaling of damaged media. International Journal of Damage Mechanics 18: 259-282.

Carpinteri, A., Lacidogna, G. & Pugno N. 2007. Structural damage diagnosis and life-time assessment by acoustic emission monitoring. Engineering Fracture Mechanics 74: 273-289.

Carpinteri, A., Lacidogna, G. & Puzzi, S. 2009b. From criticality to final collapse: Evolution of the b-value from 1.5 to 1.0. Chaos, Solitons & Fractals 41: 843-853.

Colombo, S., Main, I.G. & Forde M.C. 2003. Assessing damage of reinforced concrete beam using ''b-value'' analysis of acoustic emission signals. Journal of Materials in Civil Engineering, ASCE 15: 280-286.

Frid ,V., Rabinovitch, A. & Bahat, D. 2003. Fracture induced electromagnetic radiation. Journal of Physics D 36: 1620-1628.

Fukui, K., Okubo, S. & Terashima, T. 2005. Electromagnetic radiation from rock during uniaxial compression testing: The effects of rock characteristics and test conditions. Rock Mech. Rock Eng., 38: 411-423.

Hudson, J. A., Crouch, S. L. & Fairhurst, C. 1972. Soft, stiff and servo-controlled testing machines: A review with reference to rock failure. Engineering Geology 6: 155-189.

Jagasivamani, V. & Iyer, K.J.L. 1988. Electromagnetic emission during the fracture of heat-treated spring steel. Mater. Lett. 6: 418-422.

Johnson, J.N. & Chéret, R. 1999. Shock waves in solids: An evolutionary perspective. Shock Waves 9: 193-200.

Kaiser, J. 1950. An investigation into the occurrence of noises in tensile tests, or a study of acoustic phenomena in tensile tests. Ph. D. dissertation, Munich (FRG), Technische Hochschule München.

Lacidogna, G., Manuello, A., Durin, G., Niccolini, G., Agosto, A. & Carpinteri, A. 2009. Acoustic and magnetic emissions as precursor phenomena in failure processes. Proc. of SEM Annual Conference & Exposition on Experimental and Applied Mechanics, Albuquerque, 1-4 June 2009. Paper No. 540.

Larcher, M. 2009. Development of discrete cracks in concrete loaded by shock waves. International Journal of Impact Engineering 36: 700-710.

Miroshnichenko, M. & Kuksenko, V. 1980. Study of electromagnetic pulses in initiation of cracks in solid dielectrics. Soviet Physics-Solid State 22: 895-896.

Misra, A. 1977. Theoretical study of the fracture-induced magnetic effect in ferromagnetic materials. Physics Letters 62A: 234-236.

Misra, A. 1978. A physical model for the stress-induced electromagnetic effect in metals. Applied Physics 16: 195-199.

Ohtsu, M. 1996. The history and development of acoustic emission in concrete engineering. Magazine of Concrete Research 48: 321-330.

O'Keefe, S. G. & Thiel, D. V. 1995. A mechanism for the production of electromagnetic radiation during fracture of brittle materials. Phys. Earth Plant. Inter. 89: 127-135.

Pollock, A.A. 1973. Acoustic emission-2: Acoustic emission amplitudes. Non-Destructive Testing 6: 264–269.

Rabinovitch, A., Frid, V. & Bahat, D. 2007. Surface oscillations. A possible source of fracture induced electromagnetic oscillations. Tectonophysics 431: 15-21.

Rao, M.V.M.S. & Lakschmi, P.K.J. 2005. Analysis of b-value and improved b-value of acoustic emissions accompanying

rock fracture. Current Science-Bangalore 89: 1577-1582.
Richter, C.F. 1958. Elementary Seismology. San Francisco & London: W. H. Freeman & Company.
Rundle, J.B., Turcotte, D.L., Shcherbakov, R., Klein, W. & Sammis, C. 2003. Statistical physics approach to understanding the multiscale dynamics of earthquake fault systems. Reviews of Geophysics 41: 1-30.
Schiavi, A., Niccolini, G., Tarizzo, P., Lacidogna, G., Manuello, A. & Carpinteri, A. 2009. Analysis of acoustic emission at low frequencies in brittle materials under compression. Proc. of SEM Annual Conference & Exposition on Experimental and Applied Mechanics, Albuquerque, 1-4 June 2009. Paper No. 539.
Shiotani, T., Yuyama, S., Li, Z. W. & Othsu, M. 2000. Quantitative evaluation of fracture process in concrete by the use of improved b-value. 5th Int. Symposium on Non-Destructive Testing in Civil Engineering, Eds. Elsevier Science, Amsterdam 293-302.